AFRL-RZ-WP-TR-2011-2061

STUDIES OF INTERLEAVED DC-DC BOOST CONVERTERS WITH COUPLED INDUCTORS

James Scofield, Seana McNeal, Brett Jordan
AFRL-RZPE

Hiroyuki Kosai
UES, Inc.

Biswajit Ray
Bloomsburg University

APRIL 2011
Final Report

Approved for public release; distribution unlimited

AIR FORCE RESEARCH LABORATORY
PROPULSION DIRECTORATE
WRIGHT-PATTERSONAIR FORCE BASE, OH 45433-7251
AIR FORCE MATERIEL COMMAND
UNITED STATES AIR FORCE

NOTICE AND SIGNATURE PAGE

Using Government drawings, specifications, or other data included in this document for any purpose other than Government procurement does not in any way obligate the U.S. Government. The fact that the Government formulated or supplied the drawings, specifications, or other data does not license the holder or any other person or corporation; or convey any rights or permission to manufacture, use, or sell any patented invention that may relate to them.

This report was cleared for public release by the USAF 88th Air Base Wing (88 ABW) Public Affairs (AFRL/PA) Office and is available to the general public, including foreign nationals. Copies may be obtained from the Defense Technical Information Center (DTIC) (http://www.dtic.mil).

AFRL-RZ-WP-TR-2011-2061 HAS BEEN REVIEWED AND IS APPROVED FOR PUBLICATION IN ACCORDANCE WITH ASSIGNED DISTRIBUTION STATEMENT.

*//Signature//
JAMES D. SCOFIELD, Ph.D.
Project Engineer
Energy and Power Systems Branch
Energy/Power/Thermal Division
AFRL/RZPE

//Signature//
JOSEPH A. WEIMER, Chief
Energy and Power Systems Branch
Energy/Power/Thermal Division
AFRL/RZPE

This report is published in the interest of scientific and technical information exchange, and its publication does not constitute the Government's approval or disapproval of its ideas or findings.

*Disseminated copies will show "//signature//" stamped or typed above the signature blocks.

REPORT DOCUMENTATION PAGE

Form Approved
OMB No. 0704-0188

1. REPORT DATE *(DD-MM-YYYY)*	2. REPORT TYPE	3. DATES COVERED *(From - To)*
03-05-20111	Final Report	May 2007 – Dec 2010

4. TITLE AND SUBTITLE

Studies of Interleaved DC-DC Boost Converters with Coupled Inductors

5a. CONTRACT NUMBER
In-House

5b. GRANT NUMBER

5c. PROGRAM ELEMENT NUMBER

6. AUTHOR(S)

Hiroyuki Kosai; Seana McNeal; James Scofield; Brett Jordan; Biswajit Ray

5d. PROJECT NUMBER
3145

5e. TASK NUMBER
13

5f. WORK UNIT NUMBER
31451311

7. PERFORMING ORGANIZATION NAME(S) AND ADDRESS(ES)

AFRL/RZPE
1950 Fifth Street, Building 18, Area B
Wright-Patterson AFB, OH 45433

8. PERFORMING ORGANIZATION REPORT

9. SPONSORING / MONITORING AGENCY NAME(S) AND ADDRESS(ES)

Air Force Research Laboratory
Propulsion Directorate
Wright-Patterson AFB, OH 45433-7251
Air Force Materiel Command
United States Air Force

10. SPONSOR/MONITOR'S ACRONYM(S)

AFRL/RZPE

11. SPONSOR/MONITOR'S REPORT NUMBER(S)

AFRL-RZ-WP-TR-2011-2061

12. DISTRIBUTION / AVAILABILITY STATEMENT

Approved for public release; distribution unlimited
PA Case No: 88ABW-2011-2405

13. SUPPLEMENTARY NOTES This document contains color.

14. ABSTRACT

Interleaved power converters can be very beneficial for high performance electrical equipment applications. Reductions in size and electromagnetic emission along with an increase in efficiency, transient response, and reliability are among the many advantages to using such converters. Studies of interleaved DC-DC boost converters, which were performed by members of the Power, Energy, and Thermal Division of the Air Force Research Laboratory's (AFRL) Propulsion Directorate, included theoretical derivations and simulations, and experimental demonstrations. The experimental results showed that interleaved designs can provide significant benefit when utilized for high temperature and high power applications. In addition to the electrical performance benefits, it was also demonstrated that coupled inductor interleaved boost converters can be smaller and lighter compared to conventional converter topologies. These study results have been organized and published as several technical papers during the course of this project. In this technical report, the cumulative interleaved coupled inductor DC-DC converter studies are summarized.

15. SUBJECT TERMS:

DC-DC boost converter, coupled inductor, interleaved converter,

16. SECURITY CLASSIFICATION OF:			17. LIMITATION OF ABSTRACT	18. NUMBER OF PAGES	19a. NAME OF RESPONSIBLE PERSON
a. REPORT	b. ABSTRACT	c. THIS PAGE			James Scofield
Unclassified	Unclassified	Unclassified	SAR	21	19b. TELEPHONE NUMBER *(include area code)* 937-255-2949

Standard Form 298 (Rev. 8-98)
Prescribed by ANSI Std. 239.18

Table of Contents

Section **Page**

List of Figures

Figure **Page**

List of Tables

Table **Page**

Abstract

Interleaved power converters can be very beneficial for high performance electrical equipment applications. Reductions in size and electromagnetic emission along with an increase in efficiency, transient response, and reliability are among the many advantages to using such converters. Studies of interleaved DC-DC boost converters, which were performed by members of the Power, Energy, and Thermal Division of the Air Force Research Laboratory's (AFRL) Propulsion Directorate, included theoretical derivations and simulations, and experimental demonstrations. The experimental results clearly showed that interleaved designs can provide significant benefit when utilized for high temperature and high power applications. In addition to the electrical performance benefits, it was also demonstrated that coupled inductor interleaved boost converters can be smaller and lighter compared to conventional converter topologies. These study results have been organized and published as several technical papers during the course of this project. In this technical report, the cumulative interleaved coupled inductor DC-DC converter studies are summarized.

Introduction

Aircraft electrical systems have consistently evolved toward higher power, more compact architectures as a means to increase flight performance (e.g., thrust and maneuverability) and enhance onboard mission capability (e.g., sensors, weapons, communications) [1]. Recently, there has been a concerted effort in the aerospace industry to develop "more electric" architectures as a means to increase capability, improve reliability and maintainability, and reduce the life-cycle cost of these systems [2]. The achievement of these objectives is occurring through the subordination of mechanical, pneumatic, and hydraulic powered components by their electrically driven counterparts, most notably the flight surface control actuation subsystem. As these electrical systems have matured, thermal management requirements have become challenging, due to the contradictory effects of using higher power/thrust and increased power density, while reducing heat sinking options necessary to achieve low observability requirements. It has therefore become imperative to develop high temperature, high efficiency, and high power density electrical power systems which can reliably function during electronically extreme thermal excursions.

In response to these increasingly demanding electrical equipment power density requirements, interleaved buck and boost converters have been studied in recent years for their potential to improve power converter performance in terms of efficiency, size, conducted electromagnetic emission, and transient response. Figure 1 shows a conventional DC-DC boost converter circuit, consisting of an inductor, switch, diode, and capacitor configured in parallel to a resistive load. The inductance of inductor (L1) is *L*. For continuous current conduction mode (CCM) operation, the voltage gain between input and output voltages is given by Equation (1), where *D* is the duty ratio of switch S1.

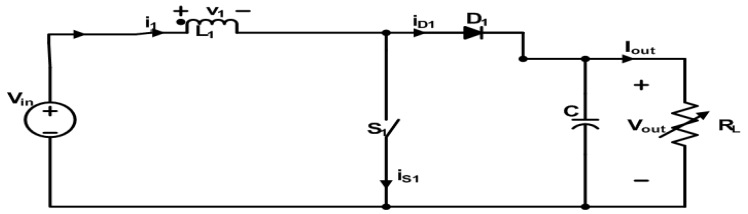

Figure 1: Conventional DC-DC Boost Converter Topology

(1) $$V_{out}/V_{in} = 1/(1-D).$$

Equation (1) reflects the fact that a large duty ratio is required for a large voltage boost, which places a practical limit on the achievable voltage step-up due to the large volume and weight of the required capacitance. For example, if the switch duty ratio (D) is greater than 0.5 (50%), the capacitor, C, supplies all of the output current for a longer portion of each period compared to the energy storage inductor. Therefore, in order to maintain acceptably small output ripple voltages, a prohibitively large capacitance is required to ensure that the output voltage does not sag as the stored energy is supplied by C during the duration D. Furthermore, since both dc and ac current are being sourced through the inductor, the inductor must be designed such that the cores will not saturate during high power operation. In addition, elevated temperatures typically lower the saturation flux threshold of the inductor core material, making this requirement a more significant design consideration. In order to address these concerns, an interleaved design involving parallel operation of two boost converters, was evaluated as a means to reduce the burden on the output capacitor as well as the form factor and weight of the inductor. Additional benefits of interleaving include high power capability, modularity, and improved reliability of the converter. An interleaved topology, however, improves converter performance at the cost of additional inductors, power switching devices, and output rectifiers. Since the inductor is the largest and heaviest component in a power boost converter, the use of a coupled inductor, where a core is shared by multiple converters instead of using multiple discrete inductors, offers a potential approach to reducing parts count, volume, and weight. Coupled inductor topologies can also provide additional advantages such as reduced core and winding loss as well as improved input and inductor current ripple characteristics. Properly implemented, the coupled inductor can also yield a decrease in electromagnetic emission, an increase in efficiency, and improved transient response. Inductor flux coupling can be realized using either direct or indirect winding configurations and is a primary design consideration for the interleaved topology. Descriptions of the benefits and disadvantages of each configuration are more fully described below.

A generalized steady state analysis of multiphase interleaved boost converters has been previously reported in detail in [3]. Useful design equations for CCM operation of an interleaved boost converter along with the effects of inductor coupling on the key converter performance parameters such as inductor ripple current, input ripple current, minimum load current requirement for achieving CCM operation are reported in [4]. Analysis of the dc and ac flux levels in the coupled inductor and its' optimization have been reported in [5]. The following sections summarize our investigations into the theory, design, and testing of interleaved DC-DC boost converters with coupled inductors. Included are discussions on a 10kW prototype, a 2kW high temperature prototype, and two 2kW compact converters that were built to demonstrate the researched concepts.

Performance analysis based on inductor coupling type

Figure 2 shows the inversely coupled interleaved DC-DC boost converter topology. For the subject DC-DC converter project, converters were primarily operated and analyzed in CCM mode so that both inductor currents (i_1 and i_2) were always positive. The primary benefit of CCM over Discontinuous Conduction Mode (DCM) of operation is the minimization of circuit ringing, inductor and input ripple current, and voltage ripple effects and their associated mitigation. A set of steady state interleaved boost converter waveforms, for CCM operation with a duty ratio greater than 0.5, are shown in Figure 3 in which input current (I_{in}), inductor voltages (V_1, V_2), inductor currents (I_1, I_2), and S1 and S2 gate drive

signals are represented. For CCM operation, the voltage gain is the same as that given for a simple boost converter described by Equation (1), ($V_{out}/V_{in} = 1/(1-D)$).

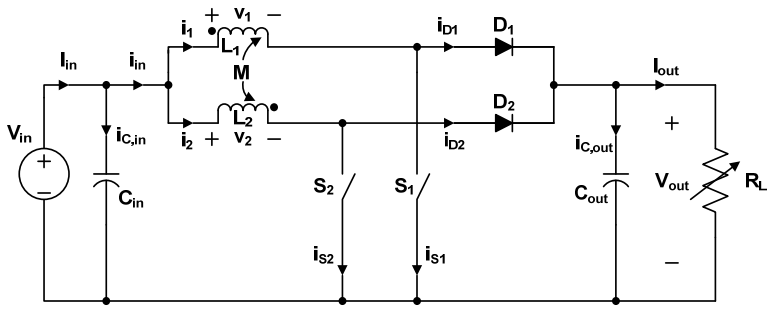

Figure 2: Inversely coupled interleaved DC-DC Boost Converter circuit

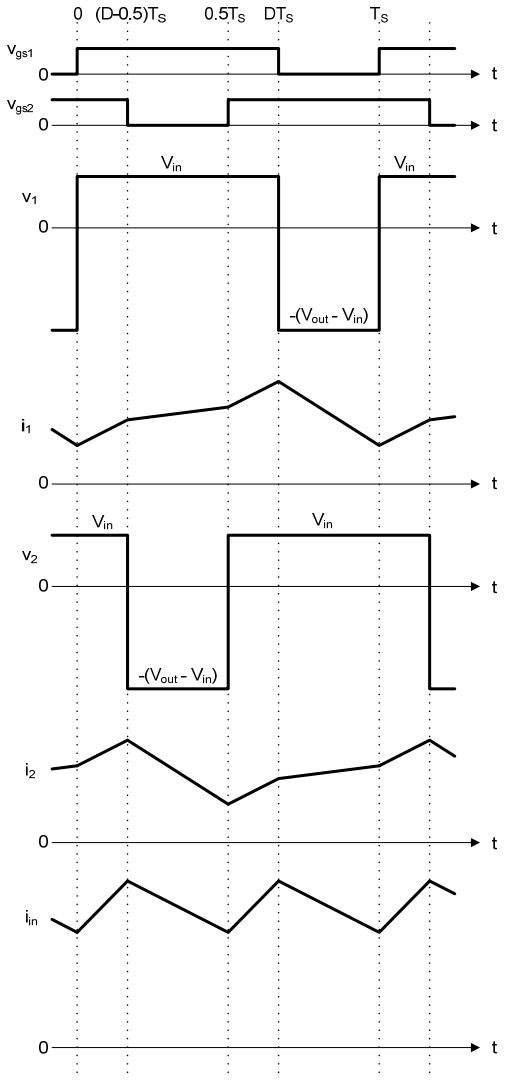

Figure 3: Theoretical Waveforms of the Interleaved Boost Converter.

A detailed analysis of converter performance based on inductor coupling configurations (direct and inverse coupled topology) is described in [4]. Equations were derived for calculating the voltage across, and current through, each of the two inductors for duty ratios of less than and greater than 50% (D< 0.5 and D> 0.5). Equivalent inductances for each of the conduction mode operating conditions were then derived and used to study the effect of coupling on inductor and input ripple currents, minimum load current requirements, and dc and ac flux levels in the inductor.

The winding configurations for coupled inductors configured for inverse and direct polarization are shown in Figure 4 along with the associated vector directions for the induced magnetic flux, B.

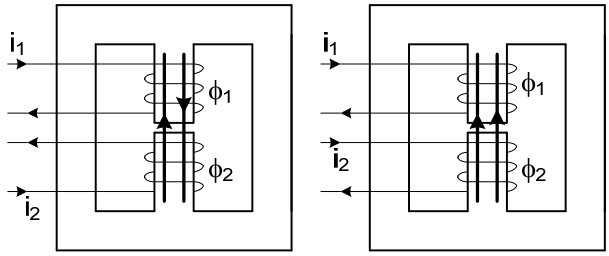

Figure 4: Winding Orientation for Inverse (left) and Direct (right) Coupled Configurations.

Inductor current and equivalent inductance analysis

The equivalent circuit for a coupled inductor is shown in Figure 5 below, illustrating its equivalence to a unity turns-ratio transformer.

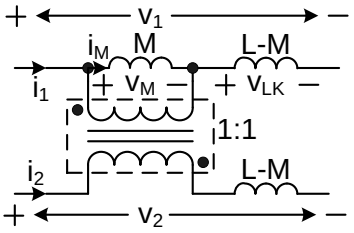

Figure 5: Transformer-like equivalent circuit of the coupled inductor

The mutual inductance is *M*, the self inductances are assumed to be equal with a value of *L*, and the coupling factor (*k)* is defined as *M/L*. The basic relationship between voltage and current for the coupled inductor is given by Equations (2) and (3).

$$v_1 = L\frac{di_1}{dt} - M\frac{di_2}{dt} \quad (2)$$

$$v_2 = L\frac{di_2}{dt} - M\frac{di_1}{dt} \quad (3)$$

The dc component of the current through each winding (I_{dc}) is given by $V_{in}/[2R_L(1-D)^2]$. Referring to Figure 3 and applying volt-sec balance to either winding of the coupled inductor yields the well-known dc voltage gain equation [$V_{out}/V_{in} = 1/(1-D)$]. Continuing this analysis, expressions for the equivalent inductance can be derived for the inverse coupled inductor configuration and are summarized in Table I for the four temporal intervals shown in Figure 3. The corresponding equivalent inductance expressions for the direct-coupled configuration are obtained by simply substituting the coupling factor *k* with *–k*. These equivalent inductances were subsequently used to predict input and inductor ripple currents as well as in determining the minimum load current condition for CCM operation (I_1, $I_2 > 0$ for all t).

Ripple current and minimum load current analysis for CCM operation

The peak-to-peak inductor ripple current is governed by the same equivalent inductance value corresponding to time interval IV for leg-1 and time interval II for leg-2. For the inverse-coupled configuration, the peak-to-peak inductor ripple current is given by

$$I_{L,ripple,p-p} = \frac{V_{out} D(1-D)}{f_s L \dfrac{1-k^2}{1-\dfrac{1-D}{D}k}}, \tag{4}$$

where f_s is the active device switching frequency.

Table I: Equivalent inductance expressions for inverse-coupled boost converter

	Time interval			
	I $\{0 \le t \le (D-0.5)T_s\}$	**II** $\{(D-0.5)T_s \le t \le 0.5T_s\}$	**III** $\{0.5T_s \le t \le DT_s\}$	**IV** $\{DT_s \le t \le T_s\}$
L_{eq1} (leg 1)	$(1-k)L$	$\dfrac{1-k^2}{1-\dfrac{D}{1-D}k}L$	$(1-k)L$	$\dfrac{1-k^2}{1-\dfrac{1-D}{D}k}L$
L_{eq2} (leg 2)	$(1-k)L$	$\dfrac{1-k^2}{1-\dfrac{1-D}{D}k}L$	$(1-k)L$	$\dfrac{1-k^2}{1-\dfrac{D}{1-D}k}L$

The corresponding inductor ripple current ratio between inverse and direct-coupling configurations is then given by (5).

$$\frac{I_{L,ripple,p-p,inverse\_coupling}}{I_{L,ripple,p-p,direct\_coupling}} = \frac{1-\frac{1-D}{D}k}{1+\frac{1-D}{D}k} \tag{5}$$

As can be seen from Table I and Equation (5), the inductor ripple current for inverse-coupling will always be less-than the direct-coupled configuration. In addition, the direct-coupled inductor ripple current becomes significantly higher as the duty and coupling ratios approach 0.5 and 1.0, respectively.

On the other hand, input ripple current is dictated by the equivalent inductance corresponding to time interval I. An expression for input ripple current for the inverse-coupled inductor configuration is given by,

$$I_{in,ripple,p-p} = \frac{2V_{out}(D-0.5)(1-D)}{f_s L(1-k)}. \tag{6}$$

Another key advantage of the inverse-coupled configuration is the ability to maintain CCM operation over a wider load (current) range compared to the direct-coupled configuration. For a given value of L, the normalized minimum load current (I_{out,min_N}) for maintaining CCM operation for the inverse-coupled configuration is given by,

$$I_{out,\min\_N} \equiv \frac{I_{out,\min}}{\left(\frac{V_{out}}{Lf_s}\right)} = \frac{D(1-D)^2\left(1-\frac{1-D}{D}k\right)}{(1-k^2)}. \tag{7}$$

The corresponding plots for both inverse and direct-coupled configurations are shown in Figure 6. It can be noted that for a given coupling ratio and a duty ratio, the CCM operation can be maintained down to a lower value of load current for the inverse-coupling case compared to the direct-coupling case.

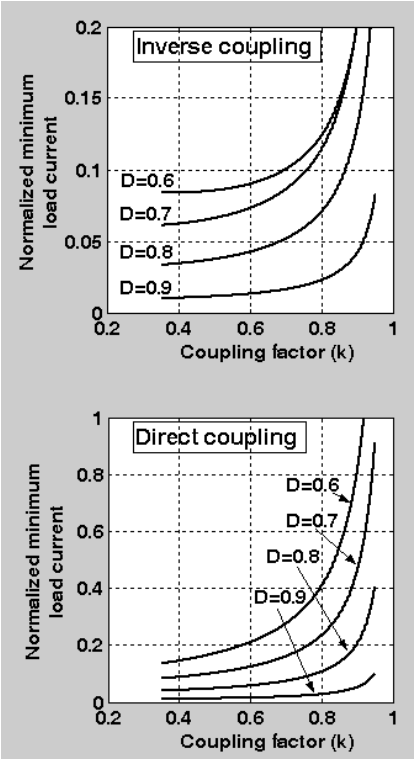

Figure 6: Normalized minimum load current for CICM operation.

Magnetic flux density analysis for CCM operation

Calculations of magnetic flux density and the associated currents that generate the flux were a primary consideration for inductor design. The basic voltage equations (1) and (2) are rearranged to derive explicit expressions for voltage across the mutual and leakage inductances. Also, an expression for the flux, ϕ_1 and ϕ_2, crossing each winding and the number of turns for each winding, N, can be expressed at the same time.

$$v_1 = N\frac{d\phi_1}{dt} = (L-M)\frac{di_1}{dt} + M\frac{d(i_1-i_2)}{dt}, \tag{8}$$

$$v_2 = N\frac{d\phi_2}{dt} = (L-M)\frac{di_2}{dt} - M\frac{d(i_1-i_2)}{dt}, \text{ and} \tag{9}$$

$$v_M = M\left(\frac{di_1}{dt} - \frac{di_2}{dt}\right). \tag{10}$$

Using the expressions above, voltages across the mutual and leakage inductances for both inverse and direct-coupled configurations can be derived. The results are shown in Table II for the same time intervals previously identified and defined in Figure 3 and Table I.

For CCM operation, the voltages across the windings are identical for both direct and inverse polarization configurations throughout the entire period; therefore the total ac magnetic flux crossing each winding is identical for both inductor configurations. The ac voltages across the windings are the sum of the voltage across the mutual inductance and the voltage across the leakage inductance. Since the induced voltage is

related to flux by Faraday's law, the mutual flux and the leakage flux across the winding can therefore be determined. The main source of flux leakage is intentionally introduced via core gaps. It should be noted that the ac flux in the core is not related to the converter's dc output current.

Table II: Voltage across mutual and leakage inductances

	Time interval			
	I $\{0 \le t \le (D-0.5)T_s\}$	**II** $\{(D-0.5)T_s \le t \le 0.5T_s\}$	**III** $\{0.5T_s \le t \le DT_s\}$	**IV** $\{DT_s \le t \le T_s\}$
v_M (Inverse coupled)	0	$\frac{kV_{in}}{(1+k)(1-D)}$	0	$-\frac{kV_{in}}{(1+k)(1-D)}$
v_M (Direct coupled)	$\frac{2kV_{in}}{(1+k)}$	$-\frac{k(2D-1)V_{in}}{(1+k)(1-D)}$	$\frac{2kV_{in}}{(1+k)}$	$-\frac{k(2D-1)V_{in}}{(1+k)(1-D)}$
v_{LK} (Inverse coupled)	V_{in}	$-\frac{(kD+D-1)V_{in}}{(1+k)(1-D)}$	V_{in}	$-\frac{(kD+D-k)V_{in}}{(1+k)(1-D)}$
v_{LK} (Direct coupled)	$\frac{V_{in}(1-k)}{(1+k)}$	$\frac{(kD+1-D)V_{in}}{(1+k)(1-D)}$	$\frac{V_{in}(1-k)}{(1+k)}$	$-\frac{(-kD+k+D)V_{in}}{(1+k)(1-D)}$

In the dc environment where two windings share dc current equally, the inverse-coupled configuration cancels the majority of the generated flux in the core due to the opposing polarity and superposition. This opposing flux configuration makes the flux in the core away from the windings substantially small. At the core directly underneath the windings, the resultant flux is $(1-k)LI_{dc}/N$, where I_{dc} is the dc current through the winding. For the direct-coupled configuration, the flux generated by two windings will sum rather than canceling within the core, which is $(1+k)LI_{dc}/N$. As a result, direct-coupling configurations will saturate the core more readily when operated at high output current conditions. The dc flux consideration represents a significant benefit to using inverse-coupled configuration in high power applications.

Useful expressions for peak-to-peak magnetic flux density, which are associated with both mutual flux and leakage flux, are shown in Table III. For these expressions, the effective cross-sectional area of the core is denoted as A_e, and the number of turns for each winding is denoted as N. It can be observed that for a given input voltage, the mutual flux density is independent of duty ratio for inverse-coupled configurations, and is duty ratio dependent for direct-coupled configurations. Additionally, the mutual flux density ratio between inverse and direct-coupled configurations is given as $1/(2D-1)$. Accordingly, the mutual flux induced core losses can be significantly higher in the inverse-coupled configuration and are a design consideration.

Table III: Currents generating mutual flux and flux density expressions for the coupled inductor

Coupling configuration	**($i_1 - i_2$) for inverse coupled ($i_1 + i_2$) for direct coupled (peak-to-peak)**	**Mutual flux density (peak-to-peak)**	**Leakage flux density (peak-to-peak)**
Inverse coupled	$\frac{kV_{in}}{M(1+k)f_s}$	$\frac{kV_{in}}{(1+k)f_s NA_e}$	$\frac{V_{in}(kD+D-k)}{(1+k)f_s NA_e}$
Direct coupled	$\frac{kV_{in}(2D-1)}{M(1+k)f_s}$	$\frac{kV_{in}(2D-1)}{(1+k)f_s NA_e}$	$\frac{V_{in}(-kD+k+D)}{(1+k)f_s NA_e}$

The results of the initial trade study confirmed the suitability of an inverse coupled winding configuration for high power converters. In addition, these results illustrated the potential benefit that systems using coupled inductors in general offer in terms of reduced magnetic component volume and weight. For the purposes of our study and potential applications of interest, inverse polarization coupling was selected as the inductor winding configuration. CCM converter operation was also chosen as design criteria for our converter based on core flux, ripple, and minimum current considerations. Attention was then focused on a suitable coupled inductor design.

Three different core geometries were analyzed, characterized, and compared in reference [5]. These different geometries produce different paths through which flux can travel. It was important to find a shape that allowed the flux to easily cancel in the air gaps i.e. desired flux leakage.

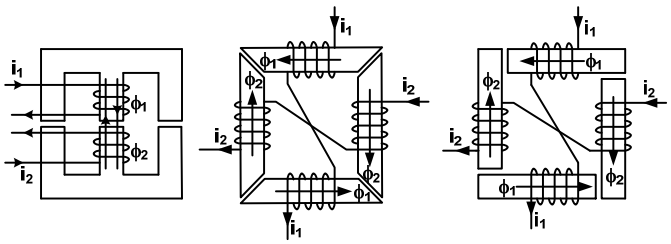

Figure 7: Winding Configuration of the Coupled Inductors.
(L to R: E-E core, square 45° gap core, and square 90° gap core)

Based on finite element analysis modeling, the square 45° gap core inductor was found to have a more uniform magnetic field throughout the core than the other inductor types. This means that the ratio of flux leakages at the gaps with respect to the total flux leakages is greatest for the square 45° gap core inductor.

The physical characteristics of the models were modified to equalize cross sectional areas, permeabilities, gap lengths, and magnetic flux path lengths of the E-E and 45° gap core inductors to that of the square 90° gap core inductor model. Since there are four gaps for both the 45° and the 90° core inductor, the two outer leg gaps of the E-E core was set to twice the gap dimension of the other two inductors. Figure 8 shows the simulated dc flux density characteristics of the three coupled inductor models during inversely coupled operation with one ampere-turn input. As can be seen in Figure 8, the E-E core produced the highest peak and average value of flux density of the three cores considered. While only a 0.2 G difference was predicted between the peak flux values of the two square cores, the 90° gap core had the

lower predicted flux density. From these simulations, verification of significant dc flux cancellation in inverse coupled configurations is confirmed, as is the apparent superiority of square geometries.

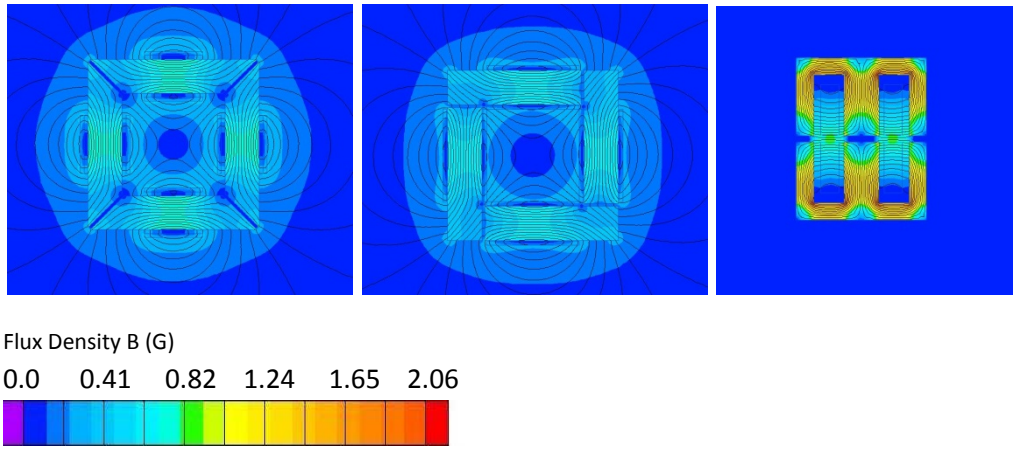

Figure 8: Flux density map for 1turn winding inductor models with 1A current. (CW from top left: square 45^{o} gap core, square 90^{o} gap core, E-E core, and legend)

Although the coupled inductors' physical characteristics were equalized for the models, their self inductances were not identical. In order to compare the models with an identical inductance (40μH), the number of windings was set to different values. Table IV shows the peak DC magnetic field/1A inside the cores for these inductors. Winding number turns for the two square coupled inductors represents the required turns wound on one core. Since windings on two opposite cores are connected in series, the actual winding turns for one of the inductors in the coupled configuration is twice the specified number of turns. The table shows that the 90 degree cut square coupled inductor cancels the DC fields best because it has the lowest peak DC magnetic field. At 270V/10kW output level, for example, the peak DC magnetic field for 90 degree cut square inductor would be about 270.1G while the E core inductor's peak DC magnetic field would be 1325G. Under the most challenging operating circumstances, such as high power and high temperature operation, DC magnetic fields can cause the inductor cores to be saturated easily. The simulation studies proved that square core inductors cancel DC fields better than E core inductors, which reduces likelihood of core saturation.

Table IV: Winding number turns and peak magnetic fields in the core for 40μH inversely polarized configured inductors.

Coupled inductor type	Windings number turns	Peak DC magnetic field (G) in the core /1A
E core	17.37	35.8
Square 45 degree cut	7.55	8.4
Square 90 degree cut	9.93	7.3

Experimental Results

Figure 9 shows a prototyped inversely coupled interleaved DC-DC converter, which was designed to operate up to 10 kW. This system consisted of six Si MOSFETS (IRFP27N60) and six SiC Schottky diodes (CSD20030D) in parallel on each leg. The MOSFETS in each boost leg were operated 180° out of phase with respect to each other. Two 30 μF X7R ceramic capacitors across the output, as well as a 30 μF X7R ceramic capacitor for a small snubber circuit across the input were used as energy storage and

voltage ripple filter elements. The ferrite core inductor was housed in a temperature controlled Teflon box. For this experiment, the load bank was at 6.75 Ω, and the input power to the DC-DC converter was generated by a 120kVA B-52 aircraft generator driven by a 350 HP drive stand. During the experiment, input and output voltages and output currents were monitored. Input current was not monitored due to lack of current probes that rated for greater than100 Adc. The gain of the converter was set to ~ 2.47. Figure 10 illustrates experimental results of input voltage, output voltage, and power data for the 10kW system. As shown in the figure, the system was successfully operated up to 10.2 kW.

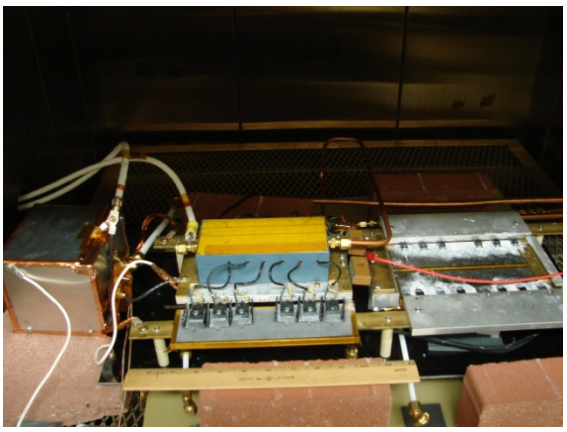

Figure 9: 10 kW Interleaved DC-DC Boost Converter inside Oven

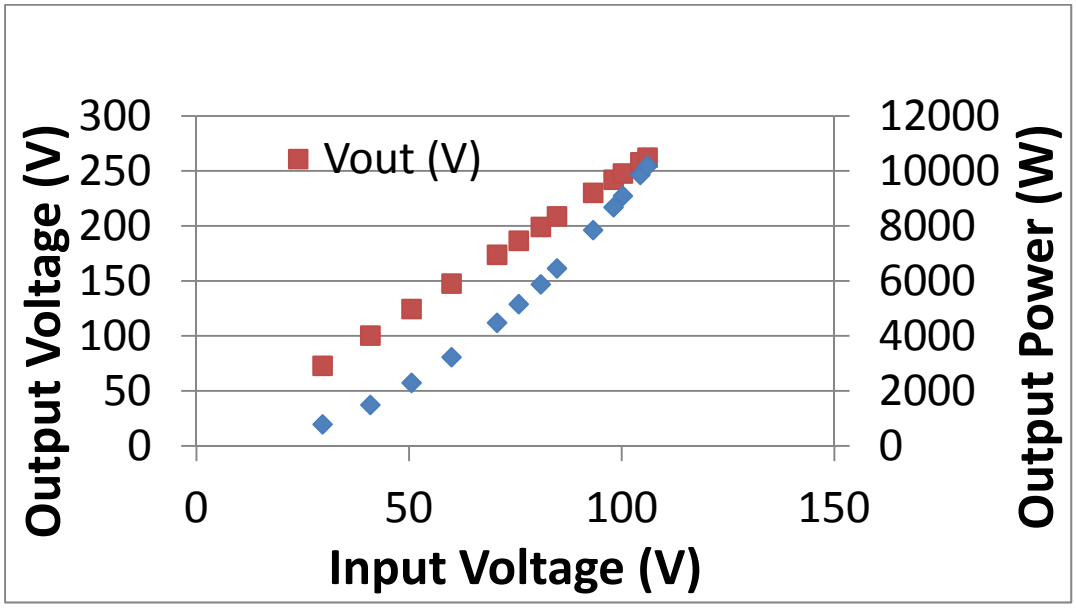

Figure 10: 10kW inversely coupled DC-DC converter. Comparison between input voltage and output voltage and current, (left) and output power with respect to output voltage.

Subsequently, a 2kW high temperature converter was designed and built to study electrical and thermal characteristics of the components from 20°C to 200°C [6]. In order to do so, this hardware, shown in Figure 11, was designed and built in a modular manner so that individual stages could be easily exchanged with replacement modules for evaluation of various candidate high temperature components. The modular design has enabled the investigation of competing switch, diode, inductor, and capacitor

technologies without redesigning/building dedicated converters for each. Si-based control circuitry was placed outside the oven and connected to the gate pins of the switches using shielded high temperature coaxial cables. With this control configuration, high temperature characteristics of the power components could be tested without a prohibitively high-cost SOI high temperature control circuit. In addition, all the solder, cables, and shielding materials used inside the oven consisted of high temperature materials capable of 200°C continuous operation.

For our high temperature DC-DC converter experimental study, SiC active devices, XPERM powdered ferrite magnetic core material, and ceramic multi-layer capacitors were used. Each leg of the interleaved converter consisted of three SiC JFETs (SJEP120R125) and three SiC Schottky diodes (CSD20030). A 90 degree corner cut square design X-perm core was fabricated as the inversely coupled inductor. The dimensions of each inductor piece were 22 mm x 17.6 mm x 67.3 mm, and the energy storage air gap at the corners was 1 mm. The measured self and mutual inductance of the coupled inductor was 39.8μH and 25.6μH, respectively. Two 30μF X7R capacitors in parallel were used as an output capacitor, and one 30μF X7R was used as the input filter.

Although the system was built with tubes for air cooling, no forced air was used during this experiment. Thus, during operation, the temperatures of all the components were above the oven temperature. The system was operated successfully without any thermal or electrical failures at elevated temperatures of up to 200°C, although changes in efficiency and V_{out} ripple were observed. Figure 12 shows the efficiencies and output voltage ripples for various oven temperatures (20°C, 100°C, 150°C, and 200°C), when the system was operated at the following condition; input voltage = 60 V, output resistance = 16 Ω, and

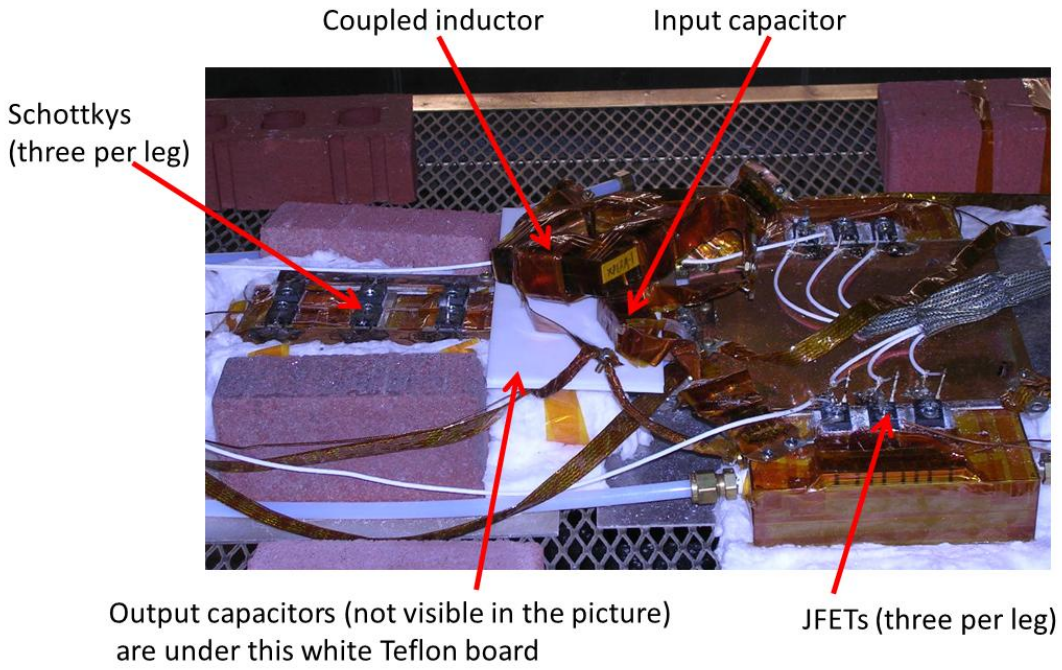

Figure 11: 2 kW High Temperature Interleaved DC-DC Boost Converter

output power =1.85 kW. As shown in this figure, prominent changes were observed for both efficiencies and V_{out} ripples above 150°C. More detailed results and analysis can be found in [6] which show the relation of the increasing ripple voltage to the degradation of capacitor parameters above 150°C.

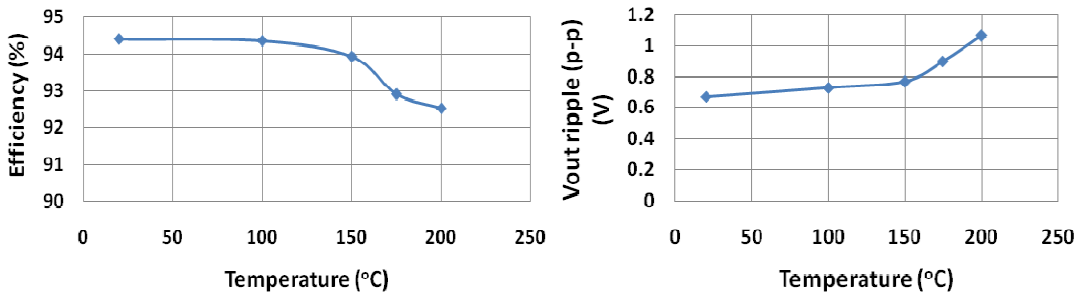

Figure 12: Efficiency vs. Temperature (left) and V_{out} ripple vs. Temperature (right) for the high temperature DC-DC converter system (input voltage = 60 V, output resistance = 16 Ω, and output power =1.85 kW).

Compact converter and high temperature capacitor test station

Since volume and weight are critical factors for airborne platforms, the next step was to take advantage of the interleaved topology and design a highly compact version of the DC-DC converter. To achieve this objective the 2 kW interleaved DC-DC boost converter was reconfigured into a more compact design. The system was enclosed in an 82 mm x 108.5 mm x 91.9 mm box. Figure 13 shows pictures of the compact converter during assembly. The top level contained the coupled inductor. A 45° coupled inductor was redesigned using four 64 mm long pieces of X-perm ferrite core material. The next level down is composed of the MOSFET switches and snubber circuits on each side, with the driver circuit in the center. The lower two levels contain the diodes and ceramic capacitors, respectively.

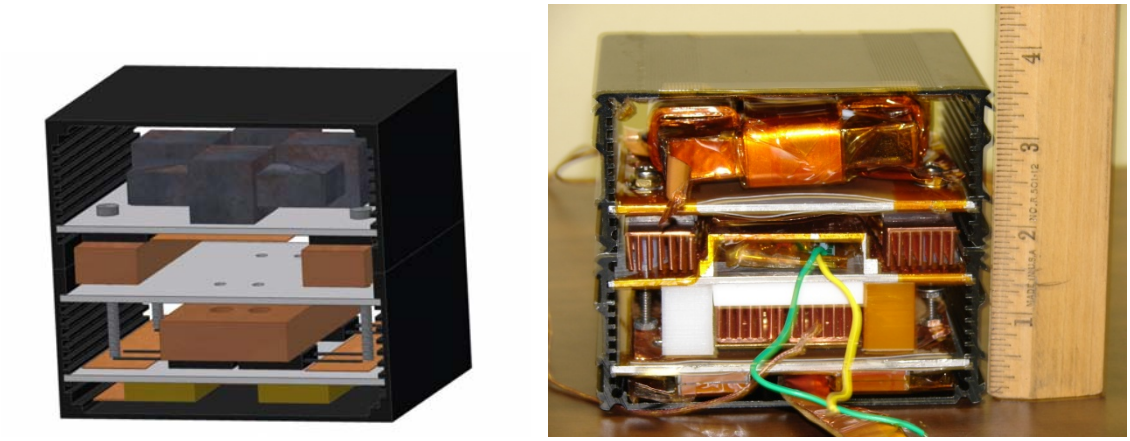

Figure 13: Compact Interleaved DC-DC Boost converter drawing (left) and actual picture (right)

Two paralleled STW45NM50 MOSFETS and two SiC Schottky diodes (CSD20030) were used for each leg. The driver circuit design remained the same while the size of the printed circuit board was reduced to about 27.6 mm by 70.1 mm. The weight of the system in the final configuration was 1.2 kg.

A similar compact interleaved DC-DC converter, as shown in Figure 14, was built as a high temperature capacitor test bed. The modular converter was placed in a sealed Teflon box (dimensions 7” x 7” x 6.5”). Teflon tubes were inserted through the Teflon box to the top level of the inner box in order to supply forced air for temperature control. Once inside, the air moved through gaps cut from the plates between the different levels in order to reach all components before exiting to the space between the inner and

outer boxes. The air was then released outside of the Teflon box through a tube. As a result, the converter's ambient temperature could be controlled between 200°C to less than 40°C even when the entire system was operating in a 200°C temperature chamber. This system is being used by the AFRL/RZPE capacitor research group to test high temperature characteristics of high power capacitors.

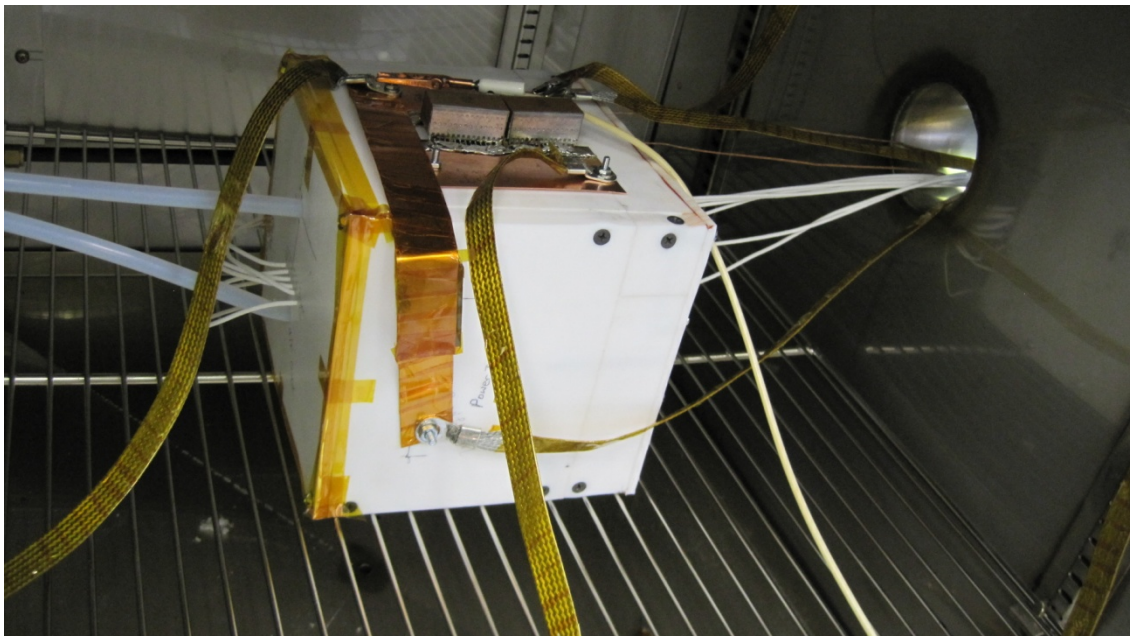

Figure 14: High temperature chamber capacitor test station using compact interleaved DC-DC converter

Conclusions

High power and high temperature studies of interleaved DC-DC converters were conducted. 10.2kW operation of the DC-DC converter demonstrated that the interleaved converter can be operated flawlessly without thermal, electrical, and EMI issues. Further, it was demonstrated that by employing high temperature components, the 2kW interleaved DC-DC converter can be easily converted to a high temperature design without increasing its size. Subsequently, a compact interleaved DC-DC boost converter was successfully constructed and demonstrated at up to 2 kW power levels. With the proper power supply and load bank setting, it is believed that the compact system could easily surpass the maximum power value previously reached. Future work will include testing other high temperature magnetic core material, novel ceramic and high temperature film capacitors, and alternative active devices such as SiC JFET and BJT's.

Reference

[1] J. Weimer, "Past Present, & Future of Aircraft Electrical Power Systems," AIAA 2001-1147.

[2] N. Shah, et al.,, "Power Management and Distribution System for More-Electric Aircraft (MADMEL)", AFRL-PR-WP-TR-2000-2043, January 2000.

[3] H. Shin et al., "Generalized steady-state analysis of multiphase interleaved boost converter with coupled inductors," *IEE Proc. Elect. Power Appl.*, Vol. 152, No. 3, pp. 584-594, May 2005.

[4] H. Kosai et al., "Characterizing the effects of inductor coupling on the performance of an interleaved boost converter," *Proc. CARTS USA 2009*, pp. 237-251, March 2009 (ISBN: 0-7908-0122-1).

[5] H. Kosai et al., “Coupled inductor characterization for a high performance interleaved boost converter,” IEEE Trans. on Magnetics, Vol. 45, No. 10, pp. 4812-4815, Oct. 2009.
[6] H. Kosai et al., “High Temperature Design and Performance Evaluation of an Interleaved Boost DC-DC Power Converter,” To be published.